Focusing properties of a modified Fibonacci photon sieve

Jie Ke (柯 杰)[1,2], Junyong Zhang (张军勇)[1,*], and Jianqiang Zhu (朱健强)[1]

[1]*Shanghai Institute of Optics and Fine Mechanics, Chinese Academy of Sciences, Shanghai 201800, China*
[2]*University of Chinese Academy of Sciences, Beijing 10049, China*
**Corresponding author: zhangjin829@163.com*

Received March 24, 2015; accepted May 27, 2015; posted online June 23, 2015

We propose a type of diffractive optical element, a modified Fibonacci photon sieve (MFiPS), designed by using the Fibonacci sequence with two different initial seed elements. Focusing properties of MFiPS show that it not only has less secondary foci, but also presents two equal intensity foci by optimizing the diameters of pinholes of MFiPS whose ratio of the two focal distances approaches the golden mean. Higher transverse resolution on the two focal spots is improved by using a super-Gaussian amplitude modulation technology.

OCIS codes: 050.1970, 340.7480, 220.4000, 230.3990.
doi: 10.3788/COL201513.080501.

Focusing of soft x-rays[1] and extreme ultraviolet (EUV) has many applications in the physical and life sciences. Unfortunately, a conventional refractive lens cannot focus soft x-rays and EUV as a consequence of the strong absorption of solid materials in the x-ray and EUV spectral regions. Traditional Fresnel zone plates (FZPs) can overcome these disadvantages[2,3], but they have inherent limitations[4]. In 2001, Kipp *et al.* proposed a photon sieve[5], where a zone plate originally composed of concentric rings is arranged properly by a large number of pinholes. Some researchers have conducted theoretical research on photon sieves[6–8], and a series of different kinds of photon sieves have been designed, such as fractal[9], compound[10], Zernike apodized[11], phase zone[12], spiral[13], and reflection[14] photon sieves. Photon sieves also have significant applications with respect to nanometer lithography[15–17], large lightweight telescopes[18], and weapons vision[19].

The Fibonacci sequence, named after the inventor and Italian mathematician Leonardo de Pisa, called Fibonacci, has been employed in the development of different photonic devices; for example, multilayers and linear grating[20], circular grating[21], spiral zone plates[22,23], and bifocal diffractive lenses[24,25].

In this Letter, we propose a modified Fibonacci photon sieve (MFiPS) to improve on-axis focusing properties by using a Fibonacci sequence with two other seed elements, which are different from the aforementioned Fibonacci lenses. Compared with a traditional photon sieve (TPS), an MFiPS consists of a large number of pinholes properly distributed over Fibonacci circular orbits. Super-Gaussian amplitude modulation technology is applied to an MFiPS in order to improve the transverse resolution of the two focal spots.

A Fibonacci photon sieve (FiPS) and an MFiPS can be constructed in a single structure without any supporting substrate, which could allow for new applications in terahertz (THz) imaging[26], x-ray microscopy[27], and ophthalmology[28], especially in bifocal intraocular or contact lenses for the correction of presbyopia.

The first two numbers of the Fibonacci sequence correspond to two seed elements $E_{-1} = A$ and $E_0 = B$, and the mth generation of the Fibonacci sequence illustrated in Fig. 1(a)[29] is obtained from the linear recursion relation $E_n = E_{n-1} + E_{n-2}$. However, the third and the fourth numbers of the Fibonacci sequence can be also chosen as initial seed elements, such as $E_1 = AA$ and $E_2 = BAB$ [see Fig. 1(c)]. In this way, some extraordinary optical focusing phenomena will appear. It should be noted that Figs. 1(a) and 1(b) are the same structure.

Figure 2 indicates how to design an FiPS in detail with seed elements $E_1 = BA$ and $E_2 = BAB$; MFiPS can be formed in the same way. If seed element A denotes potentially transparent orbits where pinholes are distributed, and B is opaque, amplitude FiPS is formed. However, if pinholes are a function of phase distribution, we can design phase FiPS and MFiPS. In this Letter, we mainly discuss the former.

FiPS and MFiPS based on the seven-order Fibonacci sequence E_7 are shown in Figs. 3(a) and 3(b). Pinholes are uniformly distributed on the potentially transparent orbits. The total number of orbits is 34 and the number

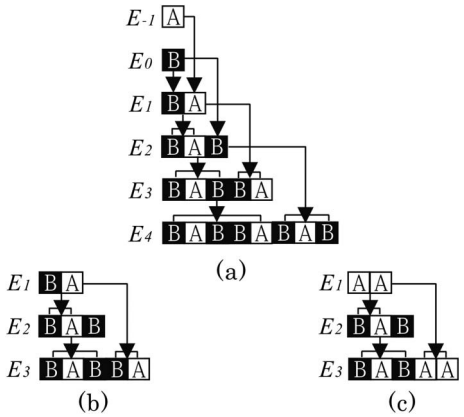

Fig. 1. Same Fibonacci sequence with different seed elements: (a) $E_{-1} = A$, $E_0 = B$; (b) $E_1 = BA$, $E_2 = BAB$; (c) $E_1 = AA$, $E_2 = BAB$.

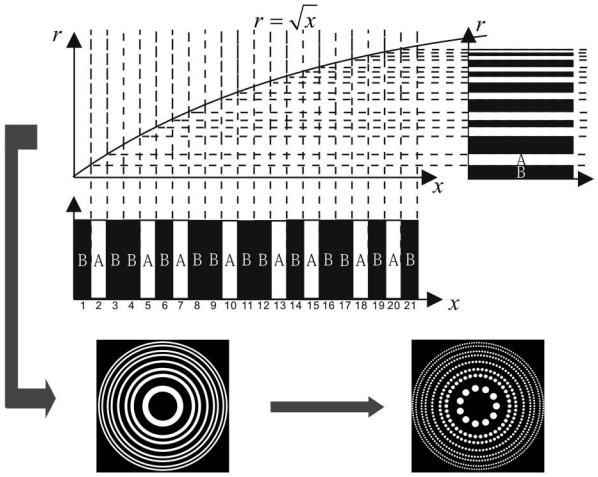

Fig. 2. Generation of FiPS.

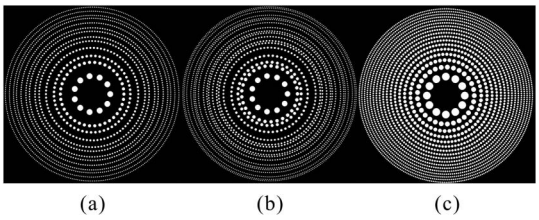

Fig. 3. (a) FiPS; (b) MFiPS; (c) TPS.

of corresponding potentially transparent orbits is 13 and 18, respectively. Figure 3(c) shows the structure of a TPS under the same condition, and the number of corresponding potentially transparent orbits is 17.

The focusing model of MFiPS is shown in Fig. 4. The MFiPS is located at the $\xi\eta$–plane, the observation plane is located at the xy–plane, and the distance between the $\xi\eta$–plane and xy–plane is z. Consider a monochromatic plane wave is incident on the nth pinhole of the mth potentially transparent orbit, whose central location and radii are denoted by (ξ_{mn}, η_{mn}) and r_{mn}, respectively. Based on the Huygens–Fresnel principle, the diffracted field $U_{mn}(x, y)$ can be given by

$$U_{mn}(x,y) = \frac{z}{i\lambda}\iint_{\Sigma} t_{mn}(\xi,\eta)\cdot\frac{\exp(ikR_{mn})}{R_{mn}^2}\mathrm{d}\xi\mathrm{d}\eta, \quad (1)$$

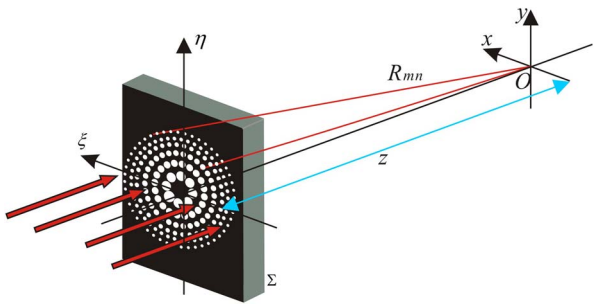

Fig. 4. Monochromatic plane wave incident on an MFiPS.

where λ is the incident wavelength, $k = 2\pi/\lambda$ is the wave number, $R_{mn} = [(x-\xi)^2 + (y-\eta)^2 + z^2]^{1/2}$ is the distance between the point $(\xi, \eta, 0)$ and the point (x, y, z), $i = (-1)^{1/2}$ is the imaginary unit, and $t_{mn}(\xi,\eta) = \mathrm{circ}\,[(\xi-\xi_{mn})/r_{mn}, (\eta-\eta_{mn})/r_{mn}]$ is the aperture function.

According to the linear superposition principle, the total diffracted field $U_{\mathrm{total}}(x, y)$ on the focal plane is the simple sum of those individual diffracted fields from different pinholes. In other words, the total diffracted field can be described as

$$U_{\mathrm{total}}(x,y) = \sum_m \sum_n U_{mn}(x,y). \quad (2)$$

The simulation parameters of TPS, FiPS, and MFiPS are as follows. The incident wavelength λ is 632.8 nm, their radii are all 3.03 mm, and the total number of orbits is 377. For TPS, the diameter d of the pinholes in each potentially transparent orbit with width w has an optimum value for the effective contribution to the prime focus in Ref. [5]. The value is given by $d = 1.53w$. Under a monochromatic plane wave illumination, the normalized axial intensity distribution produced by the TPS is shown in the dashed line in Fig. 5(a). A TPS presents only one focus which is similar to a traditional FZP and the corresponding prime focus is located at $f = 3.855$ cm. In contrast, an FiPS can present two equal intensity foci which is

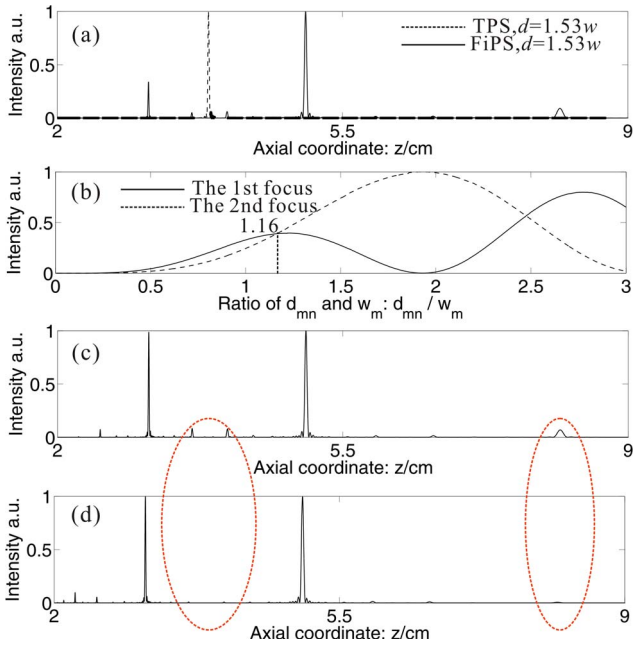

Fig. 5. Axial focusing properties of TPS, FiPS, and MFiPS: (a) normalized axial intensity produced by FiPS (solid line) and TPS (dashed line) against axial distance ($d = 1.53w$ in this case); (b) relationship of normalized axial intensity I and the value of d_{mn}/w_m at the two foci; (c) normalized axial intensity produced by FiPS against the axial distance z ($d_{mn}/w_m = 1.16$); (d) normalized axial intensity produced by MFiPS against the axial distance z.

similar to an FZP[24]. However, if we still adopt the aforementioned optimum diameter, the intensity on the two foci is not equal, as shown in the solid line in Fig. 5(a). It is demonstrated that the peak intensity of the first focus is much smaller than that of the second focus. The two axial foci are located at $f_1 = 3.120$ cm and $f_2 = 5.047$ cm. Therefore, it is imperative to again optimize the diameters of the pinholes so as to obtain two equal intensity foci.

The intensity values of the two foci of the FiPS as a function of the ratio (d_{mn}/w_m) of the diameter d_{mn} of the pinhole to the width w_m of its own orbit are plotted in Fig. 5(b). When d_{mn}/w_m values are approximately 1.16, 2.47, and so on, the first focal intensity is equal to the second focal intensity, as shown in Fig. 5(c). Unfortunately, pinholes will seriously overlap when the d_{mn}/w_m value is larger than 2. Hence, we choose 1.16 as the optimal ratio. Taking adjacent potentially transparent orbits of the MFiPS into account, there are two methods to modify the d_{mn}/w_m value so as to obtain two equal intensity foci [see Fig. 5(d)]; one is that potentially transparent orbits are divided into adjacent orbits and nonadjacent orbits in order to optimize two values of d_{mn}/w_m, and the other is that adjacent potentially transparent orbits are regarded as one orbit. In this work, we adopt the former method. In this case, the value of d_{mn}/w_m is equal to 1.00 in adjacent potentially transparent orbits, whereas the d_{mn}/w_m value in the other orbits is set to 1.19. Compared with the FiPS, the MFiPS has an outstanding axial intensity distribution with few secondary foci at the same conditions. Two focal distances of MFiPS are still 3.120 and 5.047 cm. Obviously, the ratio of two focal distances approaches the golden mean, which is one of the characteristic roots of the Fibonacci recursion relation.

The total area of the transparent pinholes is 14.206 mm^2 in the MFiPS, whereas that of the TPS is 26.429 mm^2. The diffraction efficiency of the MFiPS has fallen 9.87% compared with that of the TPS. Actually, the energy of the focal spot is just 0.2% of the incident energy[6,30] when a plane wave is incident on an amplitude TPS. One solution to improve the diffraction efficiency of the FiPS and MFiPS is to design phase FiPS and MFiPS. Figures 6(a) and 6(b) show the normalized transverse intensity distribution on the prime focal spot of the TPS. The full-width at half-maximum (FWHM) of the focal spot is 4.162 μm.

After altering the initial seed elements, the transverse resolution of MFiPS and FiPS, where the intensity of two foci is equal, is almost the same. In order to obtain higher transverse resolution, super-Gaussian amplitude modulation of pinholes which correspond to their own circular orbits is applied to the MFiPS. The weight value of a super-Gaussian amplitude modulation in the mth orbit can be described as

$$WV_m = A_m \exp\left[-\frac{(m-\mu)^M}{2\sigma^M}\right] \qquad (M \geq 2), \qquad (3)$$

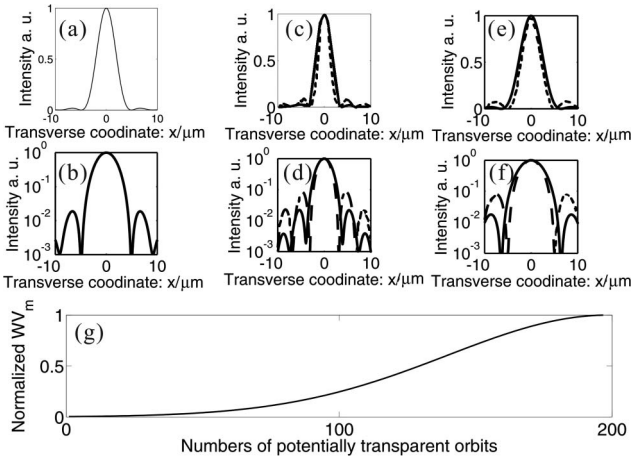

Fig. 6. (a) and (b) Normalized transverse intensity distribution on the prime focal spot of a TPS; (a) linear scale; (b) logarithmic scale; (c) and (d) normalized transverse intensity distribution on the focal spots of an unmodulated FiPS (solid line) and a modulated MFiPS (dashed line); (c) and (e) linear scale; (d) and (f) logarithmic scale; (c) and (d) first focal spot; (e) and (f) second focal spot; (g) WV_m versus number of potentially transparent orbits.

where μ and σ are the undetermined values, A_m can be either a vector or scalar, and M is the order super-Gaussian function.

Figure 6(c)–6(f) show the transverse intensity distribution of the two foci for an unmodulated FiPS (solid curves) and a modulated MFiPS (dashed curves) with super-Gaussian parameters $A_m \equiv 1$, $\mu = 377$, and $\sigma^2 = 3500$ [see Fig. 6(g)]. The FWHM of the two focal spots of the FiPS are 3.346 and 5.422 μm, whereas that of the modulated MFiPS are 2.848 and 4.604 μm. Obviously, the transverse resolution has been greatly improved.

In conclusion, we demonstrate an MFiPS with bifocal characteristics and proposed a super-Gaussian amplitude modulation approach to improve the transverse resolution of the bifocal spots. The method reported in this Letter may provide an approach for designing other MFiPSs, phase FiPS, and so on.

This work was supported by the National Natural Science Foundation of China under Grant No. 61205212 and 61205210.

References

1. Z. Chen, H. Xie, B. Deng, G. Du, H. Jiang, and T. Xiao, Chin. Opt. Lett. **12**, 123401 (2014).
2. Y. S. Chu, J. M. Yi, F. De Carlo, Q. Shen, W.-K. Lee, H. J. Wu, C. L. Wang, J. Y. Wang, C. J. Liu, C. H. Wang, S. R. Wu, C. C. Chien, Y. Hwu, A. Tkachuk, W. Yun, M. Feser, K. S. Liang, C. S. Yang, J. H. Je, and G. Margaritondo, Appl. Phys. Lett. **92**, 103119 (2008).
3. J. Kirz, J. Opt. Soc. Am. **64**, 301 (1974).
4. H. Kyurag and T. Urisu, Appl. Opt. **24**, 1139 (1985).
5. L. Kipp, M. Skibowski, R. L. Johnson, R. Berndt, R. Adelung, S. Harm, and R. Seemann, Nature **414**, 184 (2001).
6. Q. Cao and J. Jahns, J. Opt. Soc. Am. A **19**, 2387 (2002).
7. Q. Cao and J. Jahns, J. Opt. Soc. Am. A **20**, 1005 (2003).
8. J. Zhang, Q. Cao, X. Lu, and Z. Lin, Chin. Opt. Lett. **8**, 256 (2010).

9. F. Giménez, J. A. Monsoriu, W. D. Furlan, and A. Pons, Opt. Express **14**, 11958 (2006).
10. C. Xie, X. Zhu, H. Li, L. Shi, and Y. Wang, Opt. Lett. **35**, 4048 (2010).
11. G. Cheng, C. Hu, P. Xu, and T. Xing, Opt. Lett. **35**, 3610 (2010).
12. J. Jia and C. Xie, Chin. Phys. B **18**, 183 (2009).
13. C. Xie, X. Zhu, L. Shi, and M. Liu, Opt. Lett. **31**, 1756 (2010).
14. M. Kalläne, J. Buck, S. Harm, R. Seemann, K. Rossnagel, and L. Kipp, Opt. Lett. **36**, 2405 (2011).
15. R. Menon, D. Gil, G. Barbastathis, and H. I. Smith, J. Opt. Soc. Am. A **22**, 342 (2005).
16. B. Yu, W. Jia, C. Zhou, H. Cao, and W. Sun, Chin. Opt. Lett. **11**, 080501 (2013).
17. H. Ou, T.-C. Poon, K. K. Y. Wong, and E. Y. Lam, Photon. Res. **2**, 64 (2014).
18. G. Andersen and D. Tullson, Appl. Opt. **46**, 3706 (2007).
19. K. Kincade, Laser Focus World **40**, 34 (2004).
20. Y. Sah and G. S. Ranganath, Opt. Commun. **114**, 18 (1995).
21. N. Gao, Y. Zhang, and C. Xie, Appl. Opt. **50**, G142 (2011).
22. H. T. Dai, Y. J. Liu, and X. W. Sun, Proc. SPIE **8257**, 82570T (2012).
23. A. Calatayud, V. Ferrando, L. Remon, W. D. Furlan, and J. A. Monsoriu, Opt. Express **21**, 10234 (2013).
24. J. A. Monsoriu, A. Calatayud, L. Remon, W. D. Furlan, G. Saavedra, and P. Andres, IEEE Photon. J. **5**, 3400106 (2013).
25. V. Ferrando, A. Calatayud, P. Andres, R. Torroba, W. D. Furlan, and J. A. Monsoriu, IEEE Photon. J. **6**, 1 (2014).
26. T. Nagatsuma, H. Nishii, and T. Ikeo, Photon. Res. **2**, B64 (2014).
27. J. Ma, C. Yuan, G. Situ, G. Pedrini, and W. Osten, Chin. Opt. Lett. **11**, 090901 (2013).
28. T. Lu, Z. Song, Y. Su, F. Zhang, and J. Q. Yao, Chin. Opt. Lett. **5**, 475 (2007).
29. J. Hendrickson, B. C. Richards, J. Sweet, G. Khitrova, A. N. Poddubny, E. L. Ivchenko, M. Wegener, and H. M. Gibbs, Opt. Express **16**, 15382 (2008).
30. C. Hou, J. Xu, J. Bai, and G. Yang, Infrared Laser Eng. **40**, 484 (2011).